
SJTU:SPATIAL JUDGMENTS IN MULTIMODAL MODELS - TOWARDS UNIFIED SEGMENTATION THROUGH COORDINATE DETECTION *

JOONGWON CHAE^{#1}, Zhenyu Wang^{#1}, Lian Zhang^{*3}, Dongmei Yu^{*2}, Peiwu Qin^{*1}

¹Institute of Biopharmaceutical and Health Engineering, Shenzhen International Graduate School, Tsinghua University, Shenzhen, Guangdong, China, cai-zy24@mails.tsinghua.edu.cn (J. Chae)

²School of Mechanical, Electrical & Information Engineering, Shandong University, Weihai, Shandong, China

³The First Hospital of Hebei Medical University, Shijiazhuang, Hebei, China

¹These authors contributed equally to this work.

*Corresponding authors: pwqin@sz.tsinghua.edu.cn (P. Qin)

ABSTRACT

Despite significant advances in vision-language understanding, implementing image segmentation within multimodal architectures remains a fundamental challenge in modern artificial intelligence systems. Existing vision-language models, which primarily rely on backbone architectures or CLIP-based embedding learning, demonstrate inherent limitations in fine-grained spatial localization and operational capabilities. This paper introduces SJTU: Spatial Judgments in Multimodal Models - Towards Unified Segmentation through Coordinate Detection, a framework that leverages spatial coordinate understanding to bridge vision-language interaction and precise segmentation, enabling accurate target identification through natural language instructions.

The framework presents an approach for integrating segmentation techniques with vision-language models through spatial inference in multimodal space. By utilizing normalized coordinate detection for bounding boxes and transforming them into actionable segmentation outputs, we establish a connection between spatial and language representations in multimodal architectures. Experimental results demonstrate superior performance across benchmark datasets, achieving IoU scores of 0.5958 on COCO 2017 and 0.6758 on Pascal VOC. Testing on a single NVIDIA RTX 3090 GPU with 512×512 resolution images yields an average inference time of 7 seconds per image, demonstrating the framework's effectiveness in both accuracy and practical deployability. The project code is available at <https://github.com/jw-chaee/SJTU>

Keywords Vision Language Understanding, Multimodal Architecture, Spatial Coordinate Detection, Computer Vision

1 Introduction

Recent advances in multimodal models are gradually bridging the traditional gap between computer vision and natural language processing [1], yielding progress across diverse application domains. Notably, Vision-Language Models (VLMs), through their integration of visual comprehension and natural language processing capabilities [2], have demonstrated efficacy in various tasks including image caption generation [3], object recognition [4], and cross-modal retrieval [5]. Nevertheless, despite these technological strides, fundamental limitations persist in tasks requiring precise spatial understanding and segmentation.

Current approaches predominantly rely on contrastive learning-based embedding methods (e.g., CLIP [1]), which capture overall semantic associations between images and text while facing challenges in processing specific spatial relationships. Various methods have been developed to enhance spatial understanding capabilities. For instance,

**Citation: Authors. Title. Pages.... DOI:000000/11111.*

Anomaly GPT [6] employs image decoders to obtain localization results, designs dedicated prompt learners to provide fine-grained semantics for large language models, and utilizes prompt embeddings to fine-tune vision-language models. Similarly, LISA [7] adopts an image decoder architecture trained through natural language descriptions and matched images. These approaches focus on descriptive expressions for spatial understanding, where the embedding space does not explicitly preserve spatial information. These limitations affect real-world applications, such as lesion location identification in medical imaging [8], precise object manipulation in robotics [9], and object position recognition in autonomous vehicles [10]. Such applications require pixel-level precise spatial recognition rather than approximate position estimation. The absence of effective evaluation mechanisms makes it challenging to assess and improve spatial understanding capabilities during model fine-tuning processes.

Given these limitations in current approaches, it is crucial to systematically examine the fundamental challenges in spatial information processing. The precise processing of spatial information encompasses multiple fundamental challenges that warrant systematic investigation. Primarily, the maintenance of consistent spatial reference frameworks across images exhibiting heterogeneous resolutions and scale factors necessitates sophisticated calibration methodologies. Subsequently, there exists a substantial semantic-spatial translation challenge wherein models must bridge the inherent gap between natural language spatial descriptors and precise coordinate-based representations. Furthermore, the development of robust architectural frameworks that simultaneously achieve high spatial precision while maintaining generalizability across diverse operational contexts presents significant technical complexities. These intrinsic challenges emphasize the imperative need for multimodal models to incorporate more explicit and sophisticated spatial information processing mechanisms within their architectural design.

In this study, we present SJTU: Spatial Judgments in Multimodal models - Towards Unified Segmentation through Coordinate Detection, a novel framework that addresses spatial localization challenges in vision-language tasks by representing spatial information through explicit coordinate systems and leveraging Vision-Language Models (VLMs) [2] to transform natural language descriptions into standardized coordinates. The framework incorporates the Qwen2 Vision-Language model (Qwen2-VL) model [11] for processing user prompts and extracting spatial information, while integrating Segment Anything Model 2 (SAM2) [12] for segmentation tasks. Through the implementation of a standardized coordinate system, SJTU ensures consistent spatial reference across varying image resolutions, aiming to achieve precise object segmentation and offering an end-to-end solution for natural language-guided visual tasks.

The main contributions of this work are summarized as follows:

- We propose a novel methodology that effectively bridges Vision Language Models (VLMs) and segmentation techniques through coordinate-based spatial reasoning.
- We implement consistent spatial referencing through a normalized coordinate system, wherein the integration of Qwen2-VL and SAM2 enables precise object detection and segmentation.
- We validate the efficacy of our proposed method through extensive experimental evaluation on COCO 2017 and Pascal VOC datasets.

This study aims to explore the role of spatial understanding in multimodal models and suggests potential approaches to address current limitations in vision-language models. The remainder of this paper is organized as follows: Section 2 examines relevant literature and theoretical foundations, Section 3 describes the proposed methodological framework, Section 4 analyzes experimental results and their implications, Section 5 discusses the future research directions, and Section 6 concludes our work.

2 Related Work

Recent advances in vision-language models and segmentation techniques have demonstrated significant strides in multimodal models. This section discusses related work across three fundamental domains: image segmentation, vision-language models and spatial understanding in visual systems.

2.1 Image Segmentation

Image segmentation has made remarkable strides through architectural innovations. Early approaches primarily centered on CNN-based architectures, where FCN [13] pioneered end-to-end learnable segmentation methods, while U-Net [14] achieved precise boundary preservation through skip connections. The DeepLab series [15] [16] advanced the field by leveraging dilated convolutions and efficient multi-scale processing. Recently, the emergence of Transformer-based architectures introduced novel perspectives to the segmentation domain, with DETR [17] demonstrating the efficacy of attention mechanisms in visual understanding. SAM [18] introduced an advancement through its prompt-based universal segmentation framework, leveraging training on billions of masks. This foundation was further enhanced by

X-Decoder [19], which integrated multiple interaction modalities, encompassing textual, audio, and scribble-based inputs.

Recent segmentation approaches have increasingly emphasized human-machine interaction paradigms. Referring segmentation approaches [20] have enabled language-guided object localization, while interactive segmentation methodologies [21] have incorporated diverse user input mechanisms. However, these approaches predominantly rely on rudimentary matching between textual and visual features, lacking explicit spatial reasoning capabilities.

2.2 Vision-Language models

Vision-language models have achieved advancements in recent years. CLIP [1] established robust visual-linguistic alignment through large-scale contrastive learning methodologies. Building upon this foundation, GPT-4V [22] and LLaVA [23] demonstrated sophisticated visual reasoning capabilities by incorporating visual features into large language models. Parallel to these developments, researchers have explored various architectural innovations for multimodal integration. Flamingo [24] pioneered learning in visual contexts through cross-attention architectures, followed by BLIP-2 [25], which proposed innovative approaches for integrating visual features into language models. Building upon these advances, works such as MiniGPT-4 [26] further enhanced the models’ few-shot capabilities through instruction tuning.

Beyond these general advancements, vision-language models have also shown promising progress in task-specific applications. While models such as Kosmos-2 [27] have advanced the field by introducing flexible interfaces for vision-centric tasks, DetGPT [28] has focused on developing capabilities in spatially-aware detection tasks. These approaches operate in semantic space, with opportunities for further exploration in coordinate-based spatial reasoning in vision-language modeling.

2.3 Spatial Understanding in Visual Systems

Spatial understanding in visual systems has undergone an evolution: from traditional approaches that relied on geometric features [29] and rule-based methodologies [30], to the development of graph-based representations [31] and spatial relationship networks for explicit spatial modeling. The integration of vision-language models with spatial understanding has opened new research directions, where LISA [7] innovatively integrates segmentation networks and language models, demonstrating the potential of combining spatial reasoning with language understanding.

3 Method

In this section, we present a detailed description of our framework architecture and its key components, including the coordinate-based spatial understanding mechanism and the integration of vision-language and segmentation models.

3.1 Overview

Inspired by recent advances in multimodal architectures, SJTU developed a coordinate-based system that integrates visual language understanding with precise segmentation. The system comprises three core components: the SAM2 encoder, SAM2 mask decoder, and Qwen2-VL’s vision-language encoder, which work collaboratively to translate natural language commands into accurate segmentation masks.

3.1.1 Vision-Language Integration

Given an input image $x_{\text{img}} \in \mathbb{R}^{H \times W \times 3}$ and text prompt x_{txt} , our dual-encoder architecture processes visual and textual inputs through parallel pathways. The image undergoes dual processing through both SAM2 and Qwen2-VL encoders:

$$f_{\text{img}}^{\text{SAM}} = E_{\text{SAM}}(x_{\text{img}}) \tag{1}$$

$$f_{\text{img}}^{\text{VL}}, f_{\text{txt}} = E_{\text{VL}}(x_{\text{img}}, x_{\text{txt}}) \tag{2}$$

where E_{SAM} represents the SAM2 vision encoder and E_{VL} denotes the Qwen2-VL encoder. Our methodology integrates SAM2’s proficiency in precise mask generation with Qwen2-VL’s capabilities in vision-language understanding through a coordinate-based mechanism.

The SAM2 pathway (E_{SAM}) employs a hierarchical vision transformer backbone for image processing, extracting fine-grained visual features optimized for segmentation tasks. Concurrently, the Qwen2-VL pathway (E_{VL}) processes both

image and text prompts, facilitating cross-modal understanding and spatial reasoning. This dual-pathway architecture enables our system to maintain both precise spatial control and semantic comprehension.

The features extracted through these distinct pathways serve complementary objectives:

- f_{img}^{SAM} is preserved for subsequent mask generation
- f_{img}^{VL} and f_{txt} are utilized for coordinate prediction via our spatial reasoning module

This architectural strategy implements distinct pathways for segmentation and understanding, wherein SAM2’s parameters remain frozen to ensure consistent feature extraction, while the Qwen2-VL component undergoes fine-tuning to optimize coordinate prediction performance.

3.1.2 Coordinate Prediction

Building upon recent advances in spatial understanding, we extend Qwen2-VL’s functionality to generate normalized coordinates for precise spatial localization. The coordinate prediction process is formulated as:

$$[x_1, y_1, x_2, y_2] = F_{VL}(f_{img}^{VL}, f_{txt}) \quad (3)$$

where F_{VL} represents the coordinate prediction function. Following common practice in object detection, the coordinates are normalized based on image dimensions:

$$x_{norm} = \frac{x_{raw}}{W}, y_{norm} = \frac{y_{raw}}{H} \quad (4)$$

where W and H represent the width and height of the input image respectively. This normalization maps raw pixel coordinates to $[0, 1]$ range, ensuring scale-invariant representation regardless of input image resolution. For instance, in an image of size 300×200 , a bounding box with raw coordinates $[30, 60, 90, 100]$ would be normalized to $[0.1, 0.3, 0.3, 0.5]$.

This normalized coordinate system ensures resolution independence while maintaining consistent spatial reference across different image scales, which simplifies integration with downstream segmentation tasks. The coordinate prediction module leverages Qwen2-VL’s cross-modal understanding capabilities to transform natural language spatial descriptions into precise coordinate representations, bridging the gap between semantic understanding and spatial localization.

3.1.3 Mask Generation

The final segmentation mask is generated through SAM2’s mask decoder. The generation process consists of two steps. First, the normalized coordinates are transformed into prompt embeddings:

$$E_{prompt} = T_{prompt}([x_1, y_1, x_2, y_2]) \in \mathbb{R}^{N \times D} \quad (5)$$

Then, the mask decoder generates the segmentation mask using the image features and prompt embeddings:

$$\hat{M} = D_{mask}(f_{img}^{SAM}, E_{prompt}) \in \mathbb{R}^{H \times W} \quad (6)$$

where D_{mask} represents SAM2’s mask decoder, T_{prompt} is the prompt encoder that transforms coordinates into embeddings, E_{prompt} represents the prompt embeddings, and \hat{M} is the predicted binary segmentation mask. The mask decoder utilizes the pre-extracted image features f_{img}^{SAM} and the encoded prompt information to generate the final segmentation mask. To maintain model stability and consistency, we keep the parameters of SAM2’s mask decoder frozen during both training and inference stages, ensuring high-quality mask generation results.

The overall architecture of our proposed system is illustrated in Fig. 1, which depicts a dual-pathway design incorporating SAM2 for mask generation and a Multi-Modal LLM for coordinate prediction.

3.1.4 Grid Enhancement Implementation

To enhance the model’s spatial comprehension, we incorporate a grid-based visual augmentation approach following Chae et al. [32]. Their work demonstrated that a 9×9 grid pattern provides an optimal balance between spatial precision

and visual clarity, achieving significant improvements in localization tasks without architectural modifications. This enhancement serves as an explicit spatial reference framework for coordinate prediction.

The implementation involves superimposing a 9×9 black grid pattern onto the input images through alpha blending, with grid lines represented by black pixels while maintaining transparency elsewhere. This approach follows the findings of [32], where this specific grid configuration demonstrated substantial improvements in spatial understanding capabilities.

The grid enhancement is integrated into the preprocessing pipeline, executed prior to both SAM2 and Qwen2-VL encoding phases. This straightforward yet effective approach provides supplementary spatial reference information while maintaining processing efficiency, directly contributing to our framework’s improved spatial understanding capabilities.

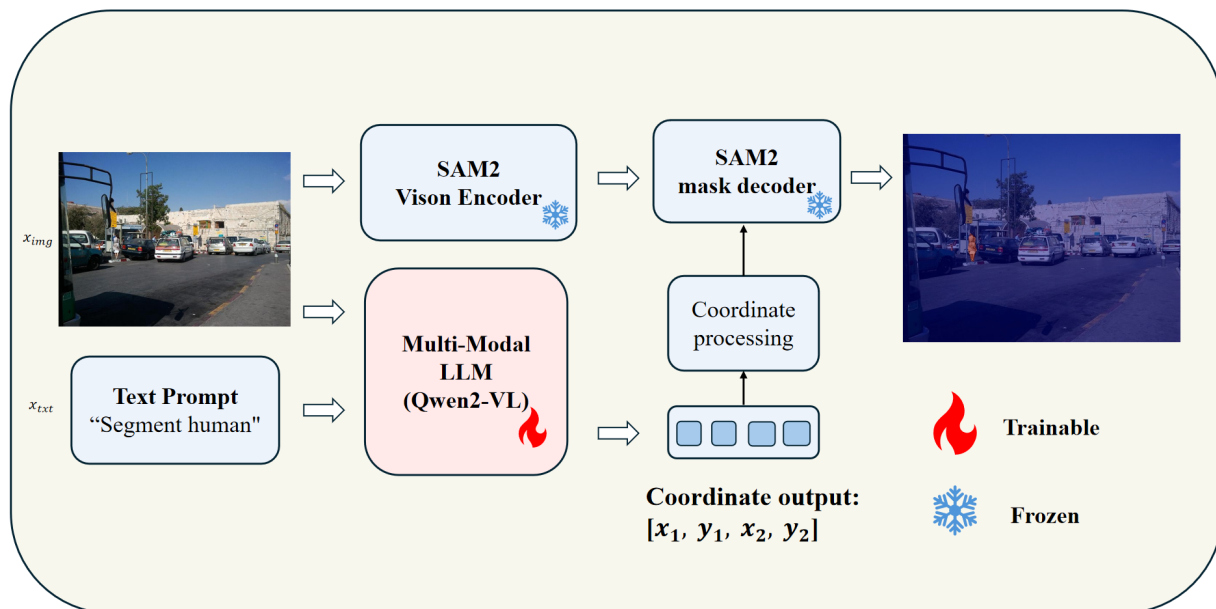


Figure 1: The overall architecture of our coordinate-based image segmentation system. The system consists of two parallel pathways: a frozen SAM2 pathway for precise mask generation and a trainable Multi-Modal LLM pathway for coordinate prediction. The input image (x_{img}) is processed by both pathways, while the text prompt (x_{txt}) is handled by the Multi-Modal LLM. The coordinate output $[x_1, y_1, x_2, y_2]$ from the LLM pathway is processed and fed into the SAM2 mask decoder to generate the final segmentation mask. The snowflake and flame icons indicate frozen and trainable components respectively.

3.2 Coordinate-based Spatial Understanding

Unlike previous approaches that rely on attention mechanisms or feature matching for spatial understanding, we introduce a coordinate-based methodology to achieve precise spatial control. This method enables end-to-end mapping from natural language instructions to precise segmentation through explicit coordinate representation and processing. Our spatial reasoning process integrates recent advances in multimodal models while incorporating novel coordinate-based control. The process initially employs Qwen2-VL for text-guided coordinate prediction, receiving natural language instructions and image input to generate normalized coordinates through multimodal understanding, outputting results in $[x_1, y_1, x_2, y_2]$ format. In the coordinate processing pipeline, the system validates predicted coordinates within the normalized range $[0, 1]$, implements resolution adaptation for consistent coordinate representation, standardizes outputs through the coordinate processing module for SAM2 mask decoder input format, and ultimately converts to pixel space coordinates for precise segmentation. This coordinate-based approach not only enables precise spatial control but also establishes a reliable localization foundation for subsequent segmentation tasks. Through the decoupling of language understanding and spatial localization, our system demonstrates enhanced capability in handling complex

vision-language interaction tasks. A detailed analysis of the VLM’s object detection capabilities is provided in Appendix A .

3.3 Model Implementation Details

In this section, we present a comprehensive analysis of the key components in our proposed framework: the SAM2-based vision encoder and mask decoder, the multi-modal large language model QWEN2-VL, and the coordinate processing module. These architecturally distinct modules work in concert to achieve end-to-end mapping from natural language descriptions to target segmentation coordinates. The SAM2 encoder is responsible for extracting high-dimensional visual features, while the QWEN2-VL model facilitates cross-modal understanding by interpreting textual prompts and interacting with visual features. The coordinate processing module subsequently transforms these multi-modal representations into precise segmentation coordinates. In the following subsections, we elaborate on the design principles and operational mechanisms of each module.

3.3.1 SAM2 Encoder Module

In this section, we elaborate on the technical details of the SAM2 encoder module. Given an input image $I \in \mathbb{R}^{H \times W \times 3}$ (where H and W denote the height and width of the image), the SAM2 vision encoder module, which builds upon the pre-trained Hierarchical architecture, extracts visual feature representations:

$$h = E(I) \in \mathbb{R}^{256 \times 64 \times 64} \quad (7)$$

where $E(\cdot)$ represents the encoder operation and h denotes the extracted feature map with dimensions of $256 \times 64 \times 64$.

The SAM2 encoder employs a multi-head attention mechanism to enhance feature representations. The core computation is formulated as:

$$Z = \text{softmax}\left(\frac{QK^T}{\sqrt{d_k}}\right)V \quad (8)$$

where Q , K , and V represent the query, key, and value matrices respectively, d_k denotes the feature dimension of the attention mechanism, and Z is the attention output. The module incorporates a memory bank M_{bank} for storing and updating feature information.

The processed features are transformed through residual connection and layer normalization to obtain the final output:

$$F_{out} = \text{LayerNorm}(\text{MLP}(Z) + h) \quad (9)$$

where F_{out} denotes the final output features, MLP represents multi-layer perceptron, and LayerNorm indicates layer normalization operation. This architectural design enables SAM2 to effectively process and integrate visual feature information.

3.3.2 SAM2 Decoder Module

The SAM2 decoder module is tightly integrated with the encoder module and is responsible for further processing the extracted features and generating the final output. The decoder leverages a multi-head attention mechanism to enhance the feature representations and optimizes the output quality through cross-layer information fusion and updates. Specifically, the decoder receives the feature map output from the encoder and applies self-attention to capture long-range dependencies within the image. This process not only aids in extracting richer contextual information but also incorporates a memory bank (M_{bank}) to store and update features, thereby enhancing the model’s memorization capabilities.

During feature processing, the decoder further refines the feature representations through residual connections and layer normalization, ensuring stability and consistency in the output. Notably, the SAM2 decoder introduces an explicit spatial coordinate integration mechanism. By incorporating spatial anchors into the model, the decoder is able to precisely handle and generate spatial information of the image, thus improving object localization accuracy and spatial understanding. Specifically, the decoder not only focuses on the feature representations but also utilizes explicit coordinate information (e.g., grid coordinates) to assist the model in better understanding the relative positions and spatial layout of objects within the image.

This design enables SAM2 to achieve superior performance in visual generation and localization tasks, enhancing spatial precision while maintaining high computational efficiency.

3.3.3 Qwen2-VL Model Module

Qwen2-VL is a multimodal model designed to effectively address the complex relationships between images and text. It achieves this by jointly learning visual and linguistic information for multimodal tasks such as visual question answering and image captioning. The computation process of the model begins with the preprocessing and feature extraction of both image and text inputs. Specifically, the input image $I \in \mathbb{R}^{H \times W \times 3}$ is divided into multiple fixed-size patches, which are then mapped into an embedding space, resulting in the embedded representation of the image patches E_{patch} :

$$E_{\text{patch}} = \text{PatchEmbed}(I) \quad (10)$$

where I represents the input image, and E_{patch} denotes the embedded representation of the image patches. These embedded image patches are subsequently processed by a visual encoder to obtain the global feature representation of the image E_{image} . The visual encoder typically employs self-attention to model the contextual relationships between the image patches:

$$E_{\text{image}} = \text{Attention}(E_{\text{patch}}) \quad (11)$$

where E_{image} represents the global feature representation of the image, and Attention refers to the self-attention mechanism that models the contextual dependencies between the image patches. Simultaneously, the text input T is tokenized and embedded into a sequence of word vectors E_{tokens} , which are then processed by a language encoder, yielding the global feature representation of the text E_{text} :

$$E_{\text{text}} = \text{Attention}(E_{\text{tokens}}) \quad (12)$$

where E_{text} represents the global feature representation of the text, and E_{tokens} refers to the tokenized word vectors. Attention is the self-attention mechanism used to capture the contextual relationships within the text. After obtaining the feature representations for both the image and the text, Qwen-VL employs a multimodal fusion mechanism to effectively combine the two sources of information. Common fusion strategies include concatenation and cross-attention. In the concatenation approach, the feature vectors E_{image} and E_{text} are directly concatenated to form a unified fusion representation:

$$E_{\text{fusion}} = \text{concat}(E_{\text{image}}, E_{\text{text}}) \quad (13)$$

where E_{fusion} represents the fused feature representation, and concat denotes the operation of concatenating the image and text feature vectors. In the cross-attention mechanism, the text features serve as the query, and the image features are used as keys and values. By computing the cross-attention, the textual information effectively guides the processing of the image features, and vice versa. The cross-attention computation is given by:

$$\text{Attention}(Q_{\text{text}}, K_{\text{image}}, V_{\text{image}}) = \text{softmax} \left(\frac{Q_{\text{text}} K_{\text{image}}^T}{\sqrt{d_k}} \right) V_{\text{image}} \quad (14)$$

where Q_{text} represents the query vector from the text, K_{image} and V_{image} represent the key and value vectors from the image, and d_k is the dimension of the keys, used to scale the dot product to prevent overflow. Softmax function normalizes the attention scores. This mechanism allows the image and text features to interact at multiple levels, further enhancing the fusion of multimodal information. Finally, the fused feature representation E_{fusion} is passed to the decoder to generate task-specific outputs. In the case of coordinate prediction tasks, the output \hat{Y} represents the predicted coordinates:

$$\hat{Y} = \text{Decoder}(E_{\text{fusion}}) \quad (15)$$

where \hat{Y} denotes the predicted coordinates, and Decoder is the component that generates task-specific outputs from the fused features. In the case of coordinate prediction tasks, the decoder generates the corresponding coordinate values based on the fused visual and textual information.

Through this multimodal learning and cross-attention mechanism, Qwen-VL is able to effectively integrate image and text information, significantly improving performance on multimodal tasks. The design architecture provides an effective solution to the deep alignment between image and text, particularly demonstrating strong expressive power and application potential in tasks such as coordinate prediction.

For efficient deployment, we utilize Activation-aware Weight Quantization (AWQ) [33] for the Qwen2-VL model. AWQ enables significant memory reduction while preserving model performance by quantizing weights to 4-bit precision while maintaining activations in FP16. This quantization strategy carefully considers activation patterns during quantization to minimize accuracy degradation, achieving an optimal balance between computational efficiency and model performance. Our implementation demonstrates that the AWQ-quantized model maintains the original model’s capabilities while significantly reducing the memory footprint and computational requirements.

3.3.4 Coordinate Processing Module

In our model architecture, the coordinate mapping module serves as a crucial link between Qwen2-VL and SAM2-decoder. Specifically, the normalized bounding box coordinates output by Qwen2-VL undergo a denormalization process before being input into the SAM2-decoder for further processing. The denormalization transformation of the normalized bounding box coordinates output by Qwen2-VL is performed using the following equations:

$$(x_p^1, y_p^1) = (x_n^1 \times W, y_n^1 \times H) \quad (16)$$

$$(x_p^2, y_p^2) = (x_n^2 \times W, y_n^2 \times H) \quad (17)$$

where (x_p^1, y_p^1) and (x_p^2, y_p^2) represent the top-left and bottom-right corners in pixel coordinates, respectively, W and H denote the image width and height, and x_n and y_n are the normalized coordinates output by Qwen2-VL. The primary function of this coordinate mapping module is to ensure that the normalized coordinates from Qwen2-VL are correctly transformed into the input format required by SAM2-decoder. This process ensures accurate cross-model data integration, thereby enhancing the model’s performance and precision in spatial localization tasks.

4 Experiments and Results

4.1 Datasets

To evaluate the effectiveness of the proposed framework, we conducted experiments on two widely used computer vision benchmarks: COCO 2017 [34] and Pascal VOC [35]. The COCO 2017 dataset, which is utilized for tasks such as object detection, instance segmentation, and image captioning, was sampled to include a subset comprising 20,000 randomly selected training images and 500 randomly chosen test images, covering 80 common object categories. The Pascal VOC dataset, another standard benchmark in computer vision, includes 1,464 fully annotated training images and 1,449 validation images, covering 20 object categories, with detailed annotations such as semantic segmentation masks and object bounding boxes.

4.2 Evaluation Metrics

To comprehensively evaluate the effectiveness of our proposed coordinate-based spatial understanding framework, we conduct thorough evaluations using multiple complementary metrics. These metrics are selected to assess both the spatial accuracy of our model’s predictions and its computational efficiency.

For spatial accuracy evaluation, we primarily utilize three variants of Intersection over Union metrics. The basic Intersection over Union (IoU) serves as our fundamental metric:

$$\text{IoU} = \frac{|B_p \cap B_{gt}|}{|B_p \cup B_{gt}|} \quad (18)$$

where B_p and B_{gt} denote the predicted and ground truth bounding boxes respectively, and $|\cdot|$ represents the area.

For a more comprehensive evaluation, we also introduce the Generalized Intersection over Union (GIoU), which provides a more nuanced evaluation by considering the smallest enclosing box:

$$\text{GIoU} = \text{IoU} - \frac{|C - (B_p \cup B_{gt})|}{|C|} \quad (19)$$

where C represents the smallest rectangular box enclosing both B_p and B_{gt} .

To achieve a comprehensive spatial assessment, we utilize the Complete Intersection over Union (CIoU), which further incorporates the distance between central points and aspect ratio consistency:

$$\text{CIoU} = \text{IoU} - \frac{\rho^2(b_p, b_{gt})}{c^2} - \alpha v \quad (20)$$

where $\rho(\cdot)$ represents the Euclidean distance between central points b_p and b_{gt} , c is the diagonal length of the smallest enclosing box, α is a positive trade-off parameter, and v measures the consistency of aspect ratio.

Beyond spatial accuracy, we also evaluate the computational efficiency through Average Inference Time (AIT), measuring the average processing time per image across our test sets.

4.3 Comparative Experiments

To compare the performance of the proposed SJTU framework with state-of-the-art vision-language segmentation models, we conducted experimental evaluations. The comparison includes seven baseline models: OVSeg, GRES, X-Decoder, SEEM, Grounded-SAM, LISA-7B, and LISA-13B. The comparison was carried out on the COCO 2017 and VOC-devkit datasets, utilizing four quantitative metrics: IoU, GIoU, CIoU, and AIT. Additionally, we investigated the impact of grid-based visual enhancement on model performance.

4.3.1 Experimental Setup

All experiments were conducted on a computing cluster equipped with single NVIDIA RTX 3090 GPUs. To ensure a fair comparison, consistent preprocessing protocols were applied across all models. For baseline evaluation, all models were tested using their official implementations and pre-trained weights.

Two experimental setups were designed: one where no grid was added to the input images, and the other where a 9×9 black grid with 0.3 transparency was overlaid on the input images to provide explicit spatial reference points, with the goal of enhancing the model’s understanding of object locations and spatial relationships.

4.3.2 Quantitative Results

The comparative results on the COCO 2017 and VOC-devkit datasets are presented in Table 1 and Table 2. Table 1 shows the performance on the original images without any grid overlay, while Table 2 presents the performance with the grid overlay applied to the images.

Method	COCO 2017			Pascal VOC			AIT (s)
	IoU	GIoU	CIoU	IoU	GIoU	CIoU	
OVSeg	0.3531	0.3328	0.3215	0.3329	0.3156	0.3047	3
GRES	0.3828	0.3656	0.3523	0.3987	0.3712	0.3695	4
X-Decoder	0.3412	0.3235	0.3128	0.3352	0.3289	0.3056	6
SEEM	0.3389	0.3198	0.3087	0.3218	0.3065	0.2923	8
Grounded-SAM	0.4298	0.4125	0.3998	0.4156	0.3989	0.3857	12
LISA-7B-v1	0.5229	0.5145	0.4692	0.5729	0.5341	0.5132	52
LISA-13B-v1	0.5553	0.4928	0.4803	0.6353	0.5587	0.5303	71
SJTU (ours)	0.5958	0.5661	0.5390	0.6758	0.6661	0.6341	7

Table 1: Results on the original images without any grid overlay.

As shown in Table 1 and Table 2, our SJTU framework demonstrates promising performance. The experimental results indicate that our model achieves competitive improvements over existing approaches on both COCO 2017 and VOC-devkit datasets. Furthermore, the introduction of the grid enhancement strategy leads to additional performance gains across all evaluation metrics.

Method	COCO 2017			Pascal VOC			AIT (s)
	IoU	GIoU	CIoU	IoU	GIoU	CIoU	
OVSeg	0.3589	0.3517	0.3472	0.3307	0.3273	0.3187	3
GRES	0.3885	0.3423	0.3305	0.3774	0.3507	0.3451	4
X-Decoder	0.3463	0.3315	0.3278	0.3528	0.3172	0.3167	6
SEEM	0.3440	0.3269	0.3143	0.3293	0.3166	0.2941	8
Grounded-SAM	0.4384	0.4291	0.4317	0.4155	0.4084	0.3949	12
LISA-7B-v1	0.5240	0.5177	0.4704	0.6143	0.6043	0.5881	52
LISA-13B-v1	0.5602	0.5432	0.5192	0.6615	0.6534	0.5992	71
SJTU (ours)	0.6033	0.6874	0.5812	0.6923	0.7642	0.6844	7

Table 2: Results on images overlaid with a 9×9 black grid at 30% opacity

4.3.3 Analysis

The experimental results demonstrate that our proposed model architecture achieves promising performance across evaluation metrics. The coordinate-based design and spatial relationship modeling mechanism enable the model to better comprehend and process image content, as validated by improvements in various evaluation metrics. In terms of model design, we emphasized efficiency optimization while maintaining performance, allowing SJTU to maintain an average inference time of 7 seconds, showing improvement compared to LISA-13B (71s) and LISA-7B (52s). Moreover, the introduction of the 9×9 grid strategy positively impacts model performance. This straightforward yet effective approach provides additional spatial reference information while preserving image features, facilitating coordinate prediction and spatial relationship understanding. Testing on both COCO 2017 and VOC-devkit datasets shows stable performance, reflecting the reliability of our proposed design approach. The experimental results indicate that our proposed model architecture achieves performance improvements while maintaining computational efficiency through optimized design and appropriate enhancement strategies. The combination of coordinate-based spatial understanding mechanisms and structured visual cues provides an effective solution for image segmentation tasks.

4.4 Segmentation Visualization

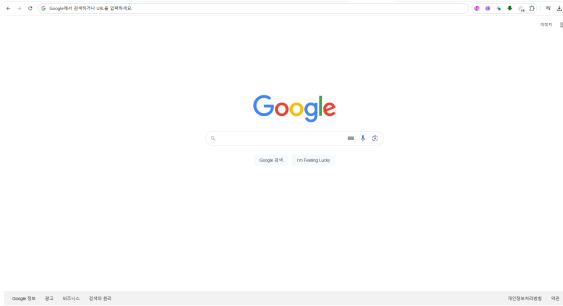
To demonstrate the effectiveness of our approach, we present qualitative results of our SJTU model’s segmentation performance. Figure 2 shows two representative examples with different segmentation scenarios.

our model demonstrates certain segmentation capabilities. In the first example (Figures 2a and 2b), the model performs basic segmentation on search engine result pages. The segmentation masks show fundamental boundary delineation and instance separation. The second example (Figures 2c and 2d) demonstrates the model’s attempt at segmenting vehicle images, achieving some effectiveness in handling vehicle body details.

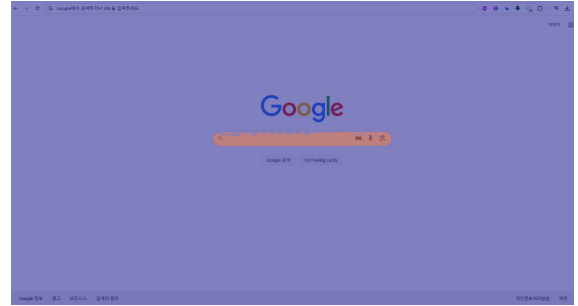
5 Discussion

In this section, we examine the current limitations and challenges of our coordinate-based spatial understanding framework, while exploring potential future research directions.

Our framework has several limitations. While our normalized coordinate system partially addresses scaling issues, the effectiveness of grid enhancement techniques is dependent on image resolution, suggesting future work could explore grid density adaptation based on image features. Additionally, the current framework primarily handles bounding box-based localization, requiring improvements in processing complex spatial relationships such as "between," "behind," and "partial occlusion." To address these limitations, we propose several future research directions. First, we can investigate adaptive grid patterns that adjust according to image content and task requirements, including varying grid densities and learnable grid patterns. Second, we can extend the coordinate system to handle complex spatial relationships and three-dimensional understanding, enabling the framework to tackle more challenging scenarios. Furthermore, exploring the integration of additional modalities such as depth information and temporal sequences could enhance the framework’s spatial understanding capabilities in complex environments.



(a) Input Image for Segment Search Engine



(b) Segmentation Result of Segment Search Engine



(c) Input Image for Segment Every Cars



(d) Segment Result of Segment Every Cars

Figure 2: Visualization of segmentation results by our SJTU model.

6 Conclusion

In this paper, we propose SJTU, a novel framework that integrates vision-language understanding and precise segmentation through coordinate-based spatial reasoning. Our experimental results demonstrate that explicit coordinate representation, augmented by grid-based visual enhancement, can effectively improve both accuracy and efficiency in multimodal segmentation tasks. Comprehensive evaluations on COCO 2017 and Pascal VOC datasets validate the efficacy of our approach, achieving competitive performance while maintaining substantially lower computational overhead compared to existing methods.

Our coordinate-based exploration presents a potential direction for vision-language interaction research, with preliminary investigations suggesting that explicit spatial representation and structured visual cues may contribute to enhanced multimodal understanding. We hope that the methodologies and insights presented in this work could serve as a modest reference for future developments in multimodal models.

References

- [1] Alec Radford, Jong Wook Kim, Chris Hallacy, Aditya Ramesh, Gabriel Goh, Sandhini Agarwal, Girish Sastry, Amanda Askell, Pamela Mishkin, Jack Clark, et al. Learning transferable visual models from natural language supervision. In *International conference on machine learning*, pages 8748–8763. PMLR, 2021.
- [2] Florian Bordes, Richard Yuanzhe Pang, Anurag Ajay, Alexander C Li, Adrien Bardes, Suzanne Petryk, Oscar Mañas, Zhiqiu Lin, Anas Mahmoud, Bargav Jayaraman, et al. An introduction to vision-language modeling. *arXiv preprint arXiv:2405.17247*, 2024.
- [3] Luowei Zhou, Hamid Palangi, Lei Zhang, Houdong Hu, Jason Corso, and Jianfeng Gao. Unified vision-language pre-training for image captioning and vqa. In *Proceedings of the AAAI conference on artificial intelligence*, volume 34, pages 13041–13049, 2020.
- [4] Jingyi Zhang, Jiaxing Huang, Sheng Jin, and Shijian Lu. Vision-language models for vision tasks: A survey. *IEEE Transactions on Pattern Analysis and Machine Intelligence*, 2024.

- [5] Haoyu Lu, Nanyi Fei, Yuqi Huo, Yizhao Gao, Zhiwu Lu, and Ji-Rong Wen. Cots: Collaborative two-stream vision-language pre-training model for cross-modal retrieval. In *Proceedings of the IEEE/CVF conference on computer vision and pattern recognition*, pages 15692–15701, 2022.
- [6] Zhaopeng Gu, Bingke Zhu, Guibo Zhu, Yingying Chen, Ming Tang, and Jinqiao Wang. Anomalygpt: Detecting industrial anomalies using large vision-language models. In *Proceedings of the AAAI Conference on Artificial Intelligence*, volume 38, pages 1932–1940, 2024.
- [7] Xin Lai, Zhuotao Tian, Yukang Chen, Yanwei Li, Yuhui Yuan, Shu Liu, and Jiaya Jia. Lisa: Reasoning segmentation via large language model. In *Proceedings of the IEEE/CVF Conference on Computer Vision and Pattern Recognition*, pages 9579–9589, 2024.
- [8] Ziyuan Qin, Huahui Yi, Qicheng Lao, and Kang Li. Medical image understanding with pretrained vision language models: A comprehensive study. *arXiv preprint arXiv:2209.15517*, 2022.
- [9] Fangchen Liu, Kuan Fang, Pieter Abbeel, and Sergey Levine. Moka: Open-vocabulary robotic manipulation through mark-based visual prompting. In *First Workshop on Vision-Language Models for Navigation and Manipulation at ICRA 2024*, 2024.
- [10] Xiaoyu Tian, Junru Gu, Bailin Li, Yicheng Liu, Yang Wang, Zhiyong Zhao, Kun Zhan, Peng Jia, Xianpeng Lang, and Hang Zhao. Drivevlm: The convergence of autonomous driving and large vision-language models. *arXiv preprint arXiv:2402.12289*, 2024.
- [11] Peng Wang, Shuai Bai, Sinan Tan, Shijie Wang, Zhihao Fan, Jinze Bai, Keqin Chen, Xuejing Liu, Jialin Wang, Wenbin Ge, et al. Qwen2-vl: Enhancing vision-language model’s perception of the world at any resolution. *arXiv preprint arXiv:2409.12191*, 2024.
- [12] Nikhila Ravi, Valentin Gabeur, Yuan-Ting Hu, Ronghang Hu, Chaitanya Ryali, Tengyu Ma, Haitham Khedr, Roman Rädle, Chloe Rolland, Laura Gustafson, et al. Sam 2: Segment anything in images and videos. *arXiv preprint arXiv:2408.00714*, 2024.
- [13] Jonathan Long, Evan Shelhamer, and Trevor Darrell. Fully convolutional networks for semantic segmentation. In *Proceedings of the IEEE conference on computer vision and pattern recognition*, pages 3431–3440, 2015.
- [14] Olaf Ronneberger, Philipp Fischer, and Thomas Brox. U-net: Convolutional networks for biomedical image segmentation. In *Medical image computing and computer-assisted intervention—MICCAI 2015: 18th international conference, Munich, Germany, October 5-9, 2015, proceedings, part III 18*, pages 234–241. Springer, 2015.
- [15] Liang-Chieh Chen. Semantic image segmentation with deep convolutional nets and fully connected crfs. *arXiv preprint arXiv:1412.7062*, 2014.
- [16] Liang-Chieh Chen. Rethinking atrous convolution for semantic image segmentation. *arXiv preprint arXiv:1706.05587*, 2017.
- [17] Nicolas Carion, Francisco Massa, Gabriel Synnaeve, Nicolas Usunier, Alexander Kirillov, and Sergey Zagoruyko. End-to-end object detection with transformers. In *European conference on computer vision*, pages 213–229. Springer, 2020.
- [18] Alexander Kirillov, Eric Mintun, Nikhila Ravi, Hanzi Mao, Chloe Rolland, Laura Gustafson, Tete Xiao, Spencer Whitehead, Alexander C Berg, Wan-Yen Lo, et al. Segment anything. In *Proceedings of the IEEE/CVF International Conference on Computer Vision*, pages 4015–4026, 2023.
- [19] Xueyan Zou, Zi-Yi Dou, Jianwei Yang, Zhe Gan, Linjie Li, Chunyuan Li, Xiyang Dai, Harkirat Behl, Jianfeng Wang, Lu Yuan, et al. Generalized decoding for pixel, image, and language. In *Proceedings of the IEEE/CVF Conference on Computer Vision and Pattern Recognition*, pages 15116–15127, 2023.
- [20] Chang Liu, Henghui Ding, and Xudong Jiang. Gres: Generalized referring expression segmentation. In *Proceedings of the IEEE/CVF conference on computer vision and pattern recognition*, pages 23592–23601, 2023.
- [21] Xi Chen, Zhiyan Zhao, Feiwu Yu, Yilei Zhang, and Manni Duan. Conditional diffusion for interactive segmentation. In *Proceedings of the IEEE/CVF International Conference on Computer Vision*, pages 7345–7354, 2021.
- [22] Zhengyuan Yang, Linjie Li, Kevin Lin, Jianfeng Wang, Chung-Ching Lin, Zicheng Liu, and Lijuan Wang. The dawn of lmms: Preliminary explorations with gpt-4v (ision). *arXiv preprint arXiv:2309.17421*, 9(1):1, 2023.
- [23] Haotian Liu, Chunyuan Li, Qingyang Wu, and Yong Jae Lee. Visual instruction tuning. *Advances in neural information processing systems*, 36, 2024.
- [24] Jean-Baptiste Alayrac, Jeff Donahue, Pauline Luc, Antoine Miech, Iain Barr, Yana Hasson, Karel Lenc, Arthur Mensch, Katherine Millican, Malcolm Reynolds, et al. Flamingo: a visual language model for few-shot learning. *Advances in neural information processing systems*, 35:23716–23736, 2022.

- [25] Junnan Li, Dongxu Li, Silvio Savarese, and Steven Hoi. Blip-2: Bootstrapping language-image pre-training with frozen image encoders and large language models. In *International conference on machine learning*, pages 19730–19742. PMLR, 2023.
- [26] Deyao Zhu, Jun Chen, Xiaoqian Shen, Xiang Li, and Mohamed Elhoseiny. Minigt-4: Enhancing vision-language understanding with advanced large language models. *arXiv preprint arXiv:2304.10592*, 2023.
- [27] Zhiliang Peng, Wenhui Wang, Li Dong, Yaru Hao, Shaohan Huang, Shuming Ma, and Furu Wei. Kosmos-2: Grounding multimodal large language models to the world. *arXiv preprint arXiv:2306.14824*, 2023.
- [28] Renjie Pi, Jiahui Gao, Shizhe Diao, Rui Pan, Hanze Dong, Jipeng Zhang, Lewei Yao, Jianhua Han, Hang Xu, Lingpeng Kong, et al. Detgpt: Detect what you need via reasoning. *arXiv preprint arXiv:2305.14167*, 2023.
- [29] David G Lowe. Distinctive image features from scale-invariant keypoints. *International journal of computer vision*, 60:91–110, 2004.
- [30] John A Bernard. Use of a rule-based system for process control. *IEEE Control Systems Magazine*, 8(5):3–13, 1988.
- [31] Jianwei Yang, Jiasen Lu, Stefan Lee, Dhruv Batra, and Devi Parikh. Graph r-cnn for scene graph generation. In *Proceedings of the European conference on computer vision (ECCV)*, pages 670–685, 2018.
- [32] Joongwon Chae, Zhenyu Wang, and Peiwu Qin. Grid-augmented vision: A simple yet effective approach for enhanced spatial understanding in multi-modal agents. *arXiv preprint arXiv:2411.18270*, 2024.
- [33] Ji Lin, Jiaming Tang, Haotian Tang, Shang Yang, Wei-Ming Chen, Wei-Chen Wang, Guangxuan Xiao, Xingyu Dang, Chuang Gan, and Song Han. Awq: Activation-aware weight quantization for on-device llm compression and acceleration. *Proceedings of Machine Learning and Systems*, 6:87–100, 2024.
- [34] Tsung-Yi Lin, Michael Maire, Serge Belongie, James Hays, Pietro Perona, Deva Ramanan, Piotr Dollár, and C Lawrence Zitnick. Microsoft coco: Common objects in context. In *Computer Vision–ECCV 2014: 13th European Conference, Zurich, Switzerland, September 6–12, 2014, Proceedings, Part V 13*, pages 740–755. Springer, 2014.
- [35] Mark Everingham, SM Ali Eslami, Luc Van Gool, Christopher KI Williams, John Winn, and Andrew Zisserman. The pascal visual object classes challenge: A retrospective. *International journal of computer vision*, 111:98–136, 2015.

A Object Detection Capability of VLM

Visual Language Models (VLMs) are multimodal models that integrate visual and language understanding capabilities. Their functionality primarily encompasses object detection and reasoning abilities. In terms of object detection, VLMs identify and locate specific targets within images, generating standardized bounding box coordinates. For reasoning capabilities, VLMs interpret natural language instructions and establish correlations between linguistic descriptions and visual content to accomplish visual understanding tasks. The integration of these capabilities enables VLMs to process user instructions and locate relevant targets in images, supporting various visual analysis tasks. As shown in the Figure 3, LLAVA and Qwen2-VL demonstrate their detection capabilities by generating bounding box coordinates in response to natural language queries.

The object detection results demonstrate the localization and reasoning capabilities of both LLAVA and Qwen2-VL. In terms of localization accuracy, LLAVA outputs coordinates [0.36,0.2,0.53,0.8], while Qwen2-VL generates coordinates [0.334,0.120,0.550,0.988]. Comparing the bounding box annotations reveals that Qwen2-VL’s detection box provides complete coverage of the target person, whereas LLAVA’s detection box fails to fully encompass the target’s upper and lower boundaries. Regarding reasoning capabilities, both models accurately interpret the instruction "president of US" and successfully locate the relevant target among multiple persons in the image while effectively excluding other individuals.

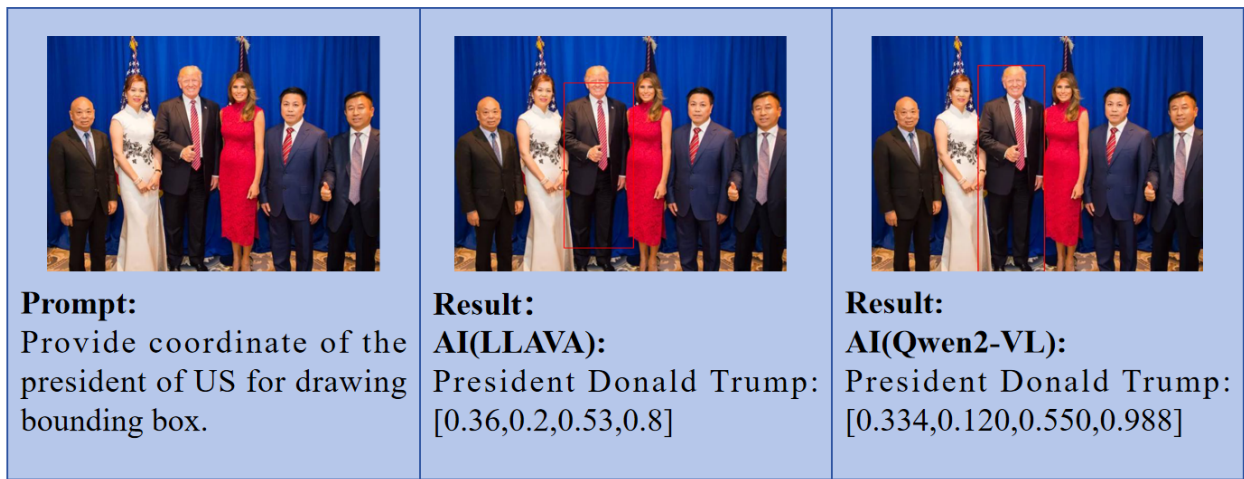


Figure 3: Detection capability comparison between LLAVA and Qwen2-VL. Both models were prompted to locate the US president in the image by providing bounding box coordinates.